Journal of Hydrology: Regional Studies 60 (2025) 102613

Contents lists available at ScienceDirect

Journal of Hydrology: Regional Studies

journal homepage: www.elsevier.com/locate/ejrh

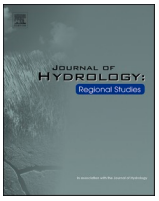

Precipitation-driven hydrological characteristics of Bei hot spring: Insights from dynamic variations of natural tracers (water discharge, water temperature, and electrical conductivity)

Yongli Guo [a,b,*], Fuxiang Chi [a,c], Qiong Xiao [a,b], Matej Blatnik [d]

[a] Institute of Karst Geology, Chinese Academy of Geological Sciences/Key Laboratory of Karst Dynamics, MNR and GZAR/International Research Center on Karst under the Auspices of UNESCO/National Center for International Research on Karst Dynamic System and Global Change, Guilin 541004, PR China
[b] Pingguo Guangxi, Karst Ecosystem, National Observation and Research Station, Pingguo, Guangxi 531406, PR China
[c] College of Earth Sciences, Guilin University of Technology, Guilin 541004, PR China
[d] Karst Research Institute, ZRC SAZU, Postojna, Slovenia

ARTICLE INFO

Keywords:
Natural tracers
Dynamic relationships
Hydrological pulse model
Hydrogeological genetic model
Bei hot spring

ABSTRACT

Study region: Bei hot spring in Chongqing, China.
Study focus: The primary objectives of this research are to analyze geothermal water characteristics of Bei hot spring, simulate the dynamic process of water discharge (Q), groundwater temperature (T_w), and electrical conductivity (EC) during the precipitation event, and build the hydrogeological genetic model for the Bei hot spring.
Results: Water flow of Bei hot spring reaches depths ranging from approximately 2.61 to 5.42 km, with the thermal reservoir temperature varying between about 72.00 and 127.36 °C. The recharge ratios of pore water, fracture water, conduit water, and hot water from the geothermal reservoir were 6.14 %, 8.86 %, and 78.63 %, respectively. The highest recession coefficient in the fracture and the relativley low conduit water ratio indicate that Bei hot spring features a less developed conduit in its upper section, along with a well-connected fracture network. The hydrological pulse model effectively simulates the dynamic variations of Q, T_w, and EC in Bei hot spring, showing a sensitive response to individual precipitation event. The catchment area of Bei hot spring, which spans 67.87 km^2, was subsequently calculated. Finally, a hydrogeological genetic model for Bei hot spring was developed, considering the spatial geological structure, water sources, and water circulation. These findings had significant implications for the assessment of water sources in karst hot springs.

1. Introduction

Chongqing, situated in southwestern China, was designated as the “the hot springs capital of China” in April 2011with, owing to its abundant thermal water resources, (Yang et al., 2017). The abundant shallow geothermal resources in Chongqing are primarily

* Corresponding author at: Institute of Karst Geology, Chinese Academy of Geological Sciences/Key Laboratory of Karst Dynamics, MNR and GZAR/International Research Center on Karst under the Auspices of UNESCO/National Center for International Research on Karst Dynamic System and Global Change, Guilin 541004, PR China.
E-mail address: ylguo89@163.com (Y. Guo).

https://doi.org/10.1016/j.ejrh.2025.102613
Received 13 February 2025; Received in revised form 23 May 2025; Accepted 11 July 2025
Available online 15 July 2025

situated within the core area of the Eastern Sichuan parallel anticline, which was formed during the Triassic-Jurassic period (Xiao et al., 2018; Zhang et al., 2022). Geothermal water is a widely available, sustainable, and scientifically viable resource among various renewable energy sources (Goswami and Rai, 2025). Geothermal water contains unique minerals that promote health (Zhang et al., 2024). The low-cost utilization of geothermal water has become a research focus for many countries worldwide (Yuan et al., 2022; Goswami and Rai, 2025). The primary focus of thermal water resource exploitation in Chongqing has been the carbonate strata located within the city's main urban area (Yang et al., 2017). The genesis and origination of thermal waters derived from carbonates exhibit a higher level of complexity than those sourced from other thermal reservoirs (Xiao et al., 2018). The thermal water resources in Chongqing encompass geothermal wells, hot springs, and geothermal mining waters (Li and Liu, 2011). The general hydrogeochemical characteristics of thermal water resources in Chongqing have been studied in the past (Xiao, 2012; Yang et al., 2017; Xiao et al., 2018). The exploitation of hot springs over the past two decades has resulted in a significant decline in both water discharge and temperature (Ta et al., 2018). Hence, it is essential to evaluate the hydrodynamics of the thermal water resources in Chongqing to uphold its status as "the hot springs capital of China". Karst hot springs represent a specific type of water outflow from karst aquifers to the surface. These hot springs, along with their associated karst aquifers, exhibit significant differences from those formed in other hydrogeological structures. The distribution of underground hot water is commonly governed by typical fracture-controlled deep circulation; however, in Chongqing, it is primarily influenced by the presence of anticlines (Ta et al., 2018), leading to an unclear recharge area for the Chongqing hot spring. Hydrological variation curves of karst aquifers have been successfully used to evaluate the precipitation infiltration coefficient and recharge area of karst aquifer system (Luo and Jiang, 2022; Li et al., 2025). Hence, the recharge zone of the typical karst hot spring in Chongqing was evaluated based on the dynamic interrelations among water discharge (Q), water temperature (T_w), and electrical conductivity (EC) of geothermal water. This assessment is vital for comprehending the water resources of karst hot springs.

There are numerous uncertainties for reliably determining the flow of underground water in karst aquifers and the related functioning of karst springs (Fiorillo et al., 2022). Groundwater temperature (T_w) is an interactive tracer whose heat changes rapidly in situations where the aquifer system recharged by mutiple water sources (conduit water, fracture water and matrix water) with different temperatures (Bonacci and Roje-Bonacci, 2023). EC values in water refers to the ability of the solution to conduct electricity and reflects the amount of total dissolved solids (TDS), it could interpret the runoff sources of karst aquifer system, and then indirectly reflect karst development characteristics of fissures and conduits (Guo et al., 2022; Shuster and White, 1971; Wang et al., 2020). Electrical conductivity (EC) and water temperature (T_w) in combination with spring discharge (Q) can reflect the infiltration pattern, the natural factors controlling the hydrochemistry and the storage characteristics (Pinza et al., 2024).

Over the past few decades, tracers such as EC, T_w, hydrochemistry, and isotopes have been employed not only to elucidate the processes of karst groundwater circulation but also to infer the spatial structural characteristics of karst aquifers (Winston and Criss, 2004; Luhmann et al., 2012; Luo et al., 2023; Guo et al., 2024). Hydrochemical ions, including Ca^{2+}, Mg^{2+}, Sr^{2+}, HCO_3^-, and SO_4^{2-}, are often employed to unravel the interactions between karst water and carbonates (Petrović and Marinović, 2023; Wei et al., 2024; Wang et al., 2025). The application of environmental isotopes, including δD, $\delta^{18}O$, and $\delta^{13}C_{DIC}$, can effectively clarify the recharge sources and flow pathways of karst groundwater (Herms et al., 2019; Guo et al., 2023). The characteristics of water flow, heat transport, and the inherent spatial structure in karst aquifers can be elucidated through the response mechanisms of EC and T_w (Birk et al., 2004; Luo et al., 2023). EC and T_w can be recored at high resolution using the Solinst Solinst (Levelogger 4.6.2 LTC, Canada), which serves as significant indicators in the process of karst groundwater circulation (Guo et al., 2024). Therefore, compared to hydrochemistry and isotopes, EC and T_w can be obatined more esaily, allowing for the interpretation of the continuous characteristics of karst groundwater dynamic and providing more stable and reliable hydrogeological information (Luo et al., 2023). The utilization of EC and T_w as natural tracers has attracted significant attention and has emerged as a widely used method for characterizing the hydrodynamics of aquifer systems (Shi et al., 2024). Time series data from natural or environmental tracers, such as EC and T_w, can be accurately recorded using dataloggers. These data are frequently used to analyze the transport characteristics of aquifer systems (Schaper et al., 2024). The hydrodynamic characteristics of the karst groundwater system are significantly influenced by the structure of the karst aquifer, which consists of conduits, fissures, and matrix (Ford and Williams, 2013). The validity of using EC and T_w as natural tracers depends on the transmission of fluctuations in these properties within the diverse medium of the karst aquifer system.

Geothermal water in Chongqing can be categorized into natural hot springs and artificial hot springs. Natural hot springs are formed when rivers erode anticlines, exposing thermal reservoirs that allow deep hot water to rise. In contrast, artificial hot springs are created by drilling into the wing or axis of to anticlines to access subterranean hot water. Compared to natural ones, Chongqing boasts a larger number of artificial hot springs, most of which feature medium to low temperatures. The deep boreholes linked to these artificial hot springs pose challenges for hydrological dynamic monitoring and complicate the assessment of water resources. Among the five renowned hot springs in Chongqing, Bei hot spring stands out as the most eminent. Since the Song dynasty, as noted by Yang et al. (2017), it has maintained a continuous operation reflecting a rich onsen culture over 1600 years, thus embodying a significant historical legacy. The outlet of the spring is well-protected and suitable for monitoring water levels, temperature, and electrical conductivity. Selecting the Bei hot spring as the research site is representative for studying the hydrodynamic mechanisms of thermal water in Chongqing. The study leveraged the dynamic interplay among precipitation-driven Q, T_w, and EC to delineate the primary determinant of hydrodynamic characteristics. It also shed light on the spatial structure of the karst hot spring, and calculated the corresponding ratios, T_w and EC values, across diverse water sources. The hydrological parameters and recharge area of the karst hot spring would be evaluated using a hydrological model simulates Q, T_w, and EC. Thus, the genetic formation model for the Bei hot spring was developed from an integrated perspective of hydrology and hydrochemistry, influenced by precipitation.

2. Field sites description

Bei hot spring (E 106°25'01.2320", N 29°51'22.8631") is located in the Bolian Hotel of Chongqing, situated on the eastern and central border of the Sichuan Basin. It is approximately 452 km from the epicenter of the Wenchuan earthquake. The outcrops of Bei hot spring are prominently exposed within the deep canyon of the main channel of the Jialingjiang river (Fig. 1 and Fig. 2). This site is situated in the steep section of the asymmetric box anticline at Wentangxia (WTX) anticline, characterized by well-developed joint fissures and faults. The water-bearing strata consist of the Leikoupo formation (T_2l), which is primarily composed of dolomitic limestone and gypsum rock, and the Jialingjiang formation (T_1j), mainly comprising brecciated dolomitic limestone, limestone, and gypsum rock (located 600–1000 m underground). Above the carbonate rocks of Leikoupo formation (T_2l) and Jialingjiang formation (T_1j) are the sandstones and shales of the upper Triassic Xujiahe formation (T_3xj), which serve to insulate water and retain heat.

The recharge area of the Bei hot spring is located in the karst outcrop region at the parallel ridge and valley anticlinal structures in eastern Sichuan and the northern end of the Huaying mountains. The EC values in Bei hot spring range from 2545.3 to 3057.0 μs/cm, which is approximately three times higher than karst shallow underground river (809.4 μs/cm). This indicates that the geothermal water primarily undergoes a long flow path and prolonged interactions between water and rocks. The thermal energy is primarily sourced from geothermal heating. The Wenchuan earthquake in 2008 disrupted several outcrops in the vicinity of the Bei hot spring (Xiao, 2012). However, the main outcrop of the Bei hot spring has remained continuously active. A automatic monitoring station was established at this outcrop to record the continous variation data of EC and T_w.

3. Materials and methods

3.1. Hydrological monitoring

To thoroughly investigate the dynamic changes in water quantity and hydrochemical characteristics of the Bei hot spring, a Solinst Levelogger 4.6.2 LTC, installed in a Marshall tank, was employed. The water temperature (T_w), electrical conductivity (EC) and water level (H_w) were measured simultaneously at 15-minute intervals, which respective accuracies of 0.01 °C, 0.1 μS/cm, and 0.01 mm. The throat width of the small Marshall tank is 0.076 m, and the equation calculation for calculating water discharge can be expressed as follows:

$$Q = 177.1 \times H_w^{1.55} \tag{1}$$

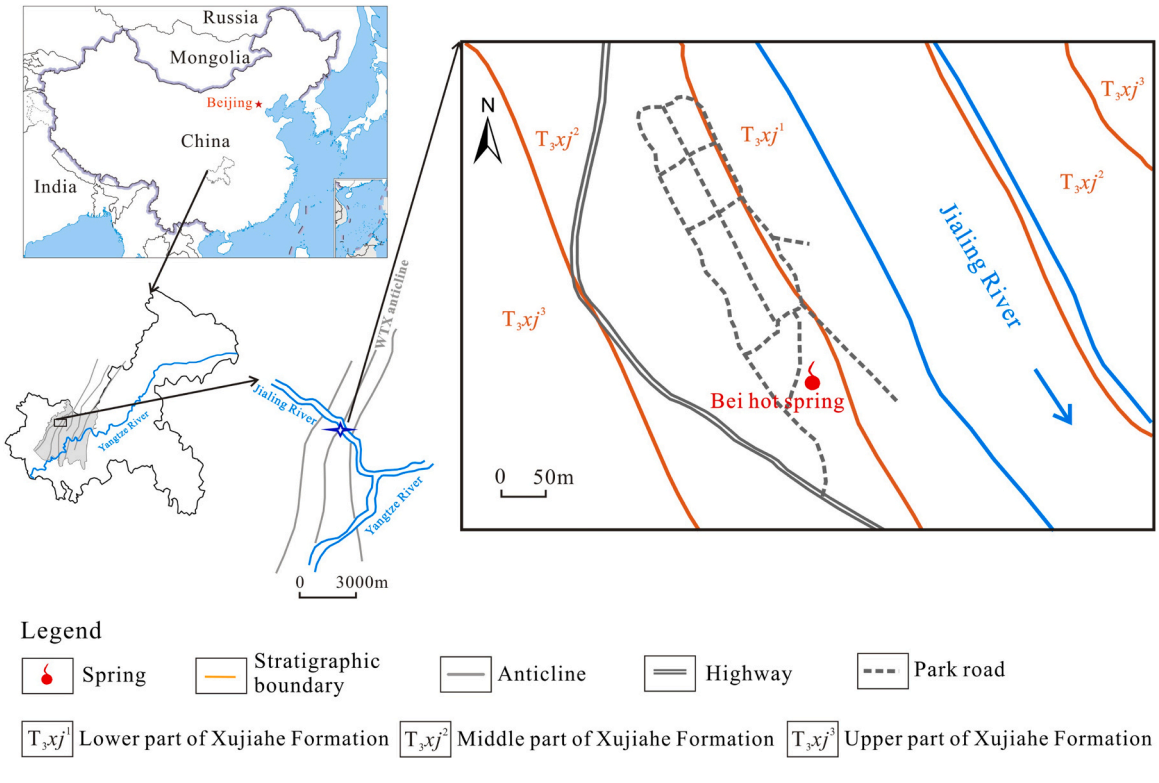

Fig. 1. The location of Bei hot spring.

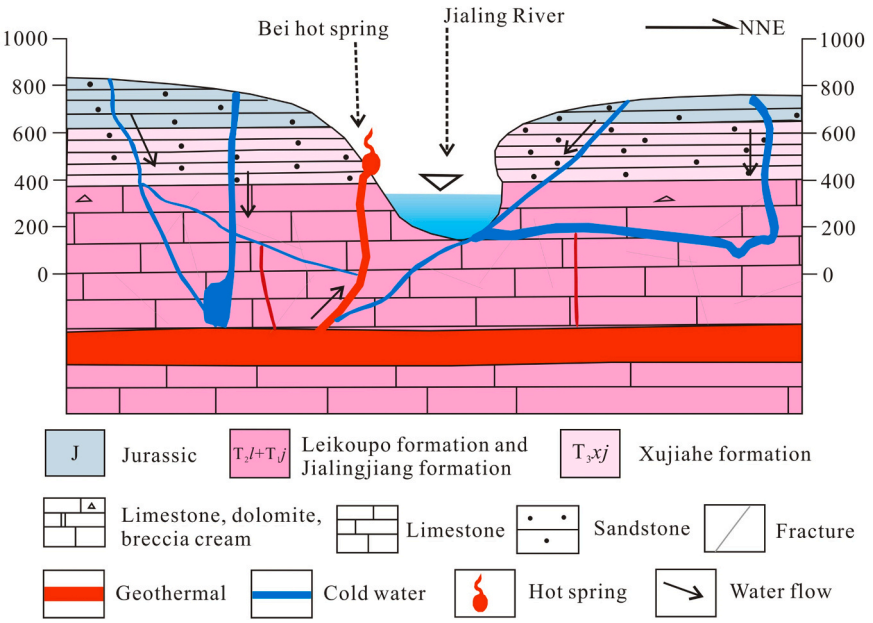

Fig. 2. Longitudinal profile of Bei hot spring.

3.2. Methods

A hydrograph is a graphical representation of variations in water discharge (Q), EC, T_w, and other hydrological variables (Bonacci and Roje-Bonacci, 2023). In comparison to isotopes and hydrochemistry, the continuously recorded Q, EC, and T_w can effectively describe the dynamic hydrological processes with high resolution. The analysis of T_w, EC, and their interaction with Q and precipitation (P) significantly enhances our understanding of the complex processes involved in water circulation and storage within the karst aquifer system.

3.2.1. The mixed ratio model based on Sr and the isotopic ratio of $^{87}Sr/^{86}Sr$

Bei hot spring is replenished by a combination of shallow cold water and hot water from the geothermal reservoir. A mixed ratio model based on Sr and the isotopic ratio of $^{87}Sr/^{86}Sr$ was employed to calculate the recharge ratios of shallow cold water and geothermal hot water. The equation used for this calculation is as follows:

$$[^{87}Sr/^{86}Sr]_{HS} \times [Sr]_{HS} = f \times ([^{87}Sr/^{86}Sr]_{SC} \times [Sr]_{SC}) + (1\text{-}f) \times ([^{87}Sr/^{86}Sr]_{GT} \times [Sr]_{GT}) \quad (2)$$

Where $[^{87}Sr/^{86}Sr]_{HS}$, $[^{87}Sr/^{86}Sr]_{SC}$, and $[^{87}Sr/^{86}Sr]_{GT}$ represent the Sr isotope ratios of hot spring, shallow cold water, and hot water from the geothermal reservoir, respectively; $[Sr]_{HS}$, $[Sr]_{SC}$, and $[Sr]_{GT}$ denote the Sr content of hot spring, shallow cold water, and hot water from the geothermal reservoir, respectively; and f indicates the recharge ratio of shallow cold water.

3.2.2. Chemical geothermometers

Chemical geothermometers include both silica geothermometers and cation geothermometers. The Na-K and K-Mg cation geothermometers demonstrate insensitivity to secondary mixing processes of thermal waters in medium- and low-temperature geothermal systems (Li et al., 2019). The water-rock interaction in the Triassic carbonate reservoir of Chongqing has not reached equilibrium (Xiao, 2012). Therefore, cation geothermometers are not reliable for assessing reservoir temperatures. Silica geothermometers primarily consist of quartz and chalcedony geothermometers. The reservoir temperature determined using chalcedony geothermometers is only slightly higher than the measured water temperature. Consequently, silica geothermometers are considered reliable for evaluating the temperatures of carbonate reservoirs.

Quartz geothermometers are categorized into three types: those with no steam loss (Eq. (3)) (Fournier, 1977), those with maximum steam loss (Eq. (4)) (Fournier, 1977), and improved quartz geothermometers (corrected) (Eq. (5)) (Verma and Santoyo, 1997). The calculations for each type are presented below:

$$T_{SiO2} = [1309/(5.19 - \log S)] - 273.15 \quad (3)$$

$$T_{SiO2} = [1522/(5.75 - \log S)] - 273.15 \quad (4)$$

$$T_{SiO2} = -44.119 + 0.24469S - 1.7414 \times 10^{-4}S^2 + 79.305 \log S \quad (5)$$

Where T_{SiO2} represents the calculated reservoir temperature, and S denotes the concentration of SiO_2 in mg/L.

3.2.3. Geothermal water circulation depth

The depth of geothermal water circulation can be calculated using the reservoir temperature (Wang et al., 1993; Ma et al., 2024). The equation for calculation is as follows:

$$Z = Z_0 + (T_R - T_0)/\Delta T \tag{6}$$

Where Z represents the depth of geothermal water circulation (m); Z_0 denotes the depth of thermostatic zone (m); T_R indicates the reservoir temperature (°C); T_0 refers to the temperature of thermostatic zone (°C); and ΔT signifies the geothermal gradient (°C/m).

3.2.4. Exponential models

The exponetial equation is a common mathematical model utilized to simulate the recession process of water discharge in karst aquifers (Maillet, 1905; Guo et al., 2024). The hydrograph recession in the karst aquifer system can be represented as the sum of three exponential components, which are described as follows (Bailly-Comte et al., 2010; Lauber et al., 2014):

$$Q_t = \begin{cases} Q_1 e^{-\alpha_1 t} [0, t_1) \\ Q_2 e^{-\alpha_2 t} [t_1, t_2) \\ Q_3 e^{-\alpha_3 t} [t_2, t_3) \end{cases} \tag{7}$$

Where Q_1, Q_2, and Q_3 represent the initial water discharge of the conduit, fracture, and matrix, respectively; α_1, α_2 and α_3 denote the recession coefficients for the conduit, fracture, and matrix, respectively.

3.2.5. Linear regression method

A simple linear regression method was employed to examine the relationship among Q, T_w, and EC in the Bei hot spring.

$$y = kx + b \tag{8}$$

In this study, T_w was identified as the independent variable (x), while EC was designated as the dependent variable (y) to analyze the dynamic variation relationships across three stages. The equation for calculating the slope value (k) is as follows:

$$k = \frac{\sum x^2 - (\sum x)^2 / n}{\sum xy - (\sum x \sum y)/n} \tag{9}$$

3.2.6. Multi-source linear mixed model

The water volume in Bei hot spring comprises conduit water, fracture water, and matrix water. Each component exhibits distinct values of water temperature and electrical conductivity. The mathematical relationships among water discharge, water temperature, and electrical conductivity in these three water components can be expressed as follows:

$$Q_C + Q_F + Q_M = Q_W \tag{10}$$

$$Q_C \times T_C + Q_F \times T_F + Q_M \times T_M = T_W \tag{11}$$

$$Q_C \times EC_C + Q_F \times EC_F + Q_M \times EC_M = EC_W \tag{12}$$

Where Q_C, Q_F, and Q_M represent the water volumes of conduit water, fracture water, and matrix water, respectively; T_C, T_F, and T_M denote the temperatures of conduit water, fracture water, and matrix water, respectively; EC_C, EC_F, and EC_M indicate the electrical conductivities of conduit water, fracture water, and matrix water, respectively. Additionally, Q_W, T_W, and EC_W represent the water volume, water temperature, and electrical conductivity at the outlet of the aquifer system, respectively.

3.2.7. Hydrological pulse model

Criss and Winston (2008) developed a hydrograph model that simulates natural hydrographs following sharp precipitation events by employing the diffusion equation and Darcy's law (Winston and Criss, 2004; Yang and Endreny, 2013; Luo et al., 2016). The calculation equations are as follows:

$$\frac{Q}{Q_p} = \left(\frac{2e\tau}{3t}\right)^{1.5} e^{-\tau/t} \tag{13}$$

$$t_p = \frac{2}{3}\tau \tag{14}$$

Where Q represents the water discharge at any given moment; Q_p denotes the peak water discharge; t signifies the elapsed time since the recharge event; e refers the Euler's number; and τ indicates the intrinsic time constant, which represents the characteristic response time of the aquifer system. The theoretical lag time between the rise of aquifer and the peak flow is given by $2\tau/3$. Additionally, t_p

represents the time of peak water discharge following the increase in water discharge.

The total water discharge (Q_{event}) resulting from the precipitation event can be determined not only by the groundwater runoff depth (i.e. effective precipitation, $P_{eff} = \alpha \times P$; where α represents the precipitation infiltration coefficient) and the catchment area (A) (Eq. (9)), but also by integrating the water discharge over time (Eq. (12)).

$$Q_{event} = \alpha \times P \times A \tag{15}$$

$$Q_{event} = Q_p \tau \sqrt{\pi} \left(\frac{2e}{3}\right)^{1.5} \tag{16}$$

By combining Eqs. (15) and (16), the resulting mathematical equation is derived:

$$Q_p = \frac{\alpha \times P \times A}{\tau \sqrt{\pi} \left(\frac{2e}{3}\right)^{1.5}} = MP \tag{17}$$

$$M = \frac{\alpha \times A}{\tau \sqrt{\pi} \left(\frac{2e}{3}\right)^{1.5}} \tag{18}$$

By combining Eqs. (13) and (15), the resulting mathematical equation is derived:

$$Q = \mathrm{MP} \left(\frac{2e\tau}{3t}\right)^{1.5} e^{-\tau/t} \tag{19}$$

The total hydrograph represents the cumulative sum of individual hydrograph elements during a series of continuous precipitation events. The total water discharge can be expressed as follows:

$$Q_t = \sum_{i=1}^{m} MP_i \left(\frac{2e\tau}{3t}\right)^{1.5} e^{-\tau/t} \tag{20}$$

Where Q_t represents the water discharge at time of t, and m denotes the number of precipitation events.

From the Eq. (15), it is clear that the value of M is determined by the linear slope value between Q_p and P_{eff}, which is influenced by the parameters of α, A, and τ.

The simulated hydrograph was compared with the observed hydrograph to calibrate the parameters τ and M, with the aim of improving both the agreement and maximizing the Nash-Sutcliffe efficiency (NSE) (Nash and Sutcliffe, 1970) and volumetric efficiency (VE) (Criss and Winston, 2008). The closer the NSE and VE are to 1, the more effective the calibration or validation results.

$$NSE = 1 - \frac{\sum_{i=1}^{n} (Q_{obs} - Q_{sim})_i^2}{\sum_{i=1}^{n} (Q_{obs} - \bar{Q}_{obs})_i^2} \tag{21}$$

$$VE = 1 - \frac{\sum_{i=1}^{n} |Q_{obs} - Q_{sim}|_i}{\sum_{i=1}^{n} (Q_{obs})_i} \tag{22}$$

Where n represents the total number of rainfall-runoff events; i is an integer varying from 1 to n; Q_{obs} denotes the observed runoff; $\bar{Q}_{obs}$ signifies the mean observed runoff; and Q_{sim} refers to the simulated runoff.

4. Results and discussion

4.1. Recharge characteristics, thermal reservoir temperature, and water circulation depth of Bei hot spring

Values of $[^{87}Sr/^{86}Sr]_{HS}$, $[^{87}Sr/^{86}Sr]_{SC}$, and $[^{87}Sr/^{86}Sr]_{GT}$ were 0.70828, 0.70830, and 0.70812, respectively. Values of $[Sr]_{HS}$, $[Sr]_{SC}$, and $[Sr]_{GT}$ were 12,250, 1632, and 15,140 μg/L, respectively. The recharge ratios of shallow cold water and hot water from the geothermal reservoir, as calculated using the Eq. (2), were 21.37 % and 78.63 %, respectively. Consequently, the Bei hot spring primarily originates from the geothermal reservoir. Shallow cold water enters the system as geothermal water flows upward through the faults and fractures. Therefore, it is essential to analyze the thermal reservoir temperature and water circulation depth to understand the hydrogeological characteristics of Bei hot spring.

Considering the subsurface thermal reservoir temperature is crucial when evaluating the potential for geothermal resource utilization. The reservoir temperature, an essential indicator of the geothermal system, thus provides a clearer reflection of the conditions at depth (Na et al., 2024). Quartz geothermometers (Fournier, 1977) have proven effective not only in alkaline thermal groundwater but also in waters with temperatures reaching up to 180 °C (Grasby et al., 2019). The SiO_2 concentration in the Bei hot spring is measured at 24.54 mg/L. The reservoir temperatures (T_R) calculated using Eqs. (3)–(5) are 71.32 °C, 127.36 °C, and 72.00 °C, respectively. The temperature variation range of the carbonate thermal reservoir in the Bei hot spring system is between 72.00 °C and

127.36 °C, further validating the suitability of quartz geothermometers for estimating the temperatures of carbonate reservoirs.

The thermostatic zone in Chongqing reaches to a depth of approximately 15 m to 40 m (Z_0), with a temperature of around 19.6°C (T_0) (Cui et al., 2011). Below this depth of 40 m, the geothermal gradient is measured at 0.02°C/m (ΔT) (Cui et al., 2011). The depth of geothermal water circulation (Z) in the Bei hot spring system, calculated using the Eq. (3), ranges from 2.61 km to 5.42 km. It can be concluded that precipitation infiltrates the exposed carbonate rock, subsequently entering the deep water cycle. As the water traverses the surrounding rock, its temperature gradually rises, ultimately emerging as a hot spring in the deep valley. The hot water from the geothermal reservoir remains relatively stable, whereas the shallow cold water is susceptible to precipitation due to its shallow water flow paths. The response characteristics of Q, T_w, and EC in the Bei hot spring in relation to precipitation would be discussed in the following sections.

4.2. Response characteristics of Q, T_w, and EC in the Bei hot spring to precipitation

4.2.1. EC and T response in Bei hot spring

The average of T_w and EC values recorded at the Bei hot spring during the monitoring period were 36.24 °C and 3011.66 μs/cm, respectively. Variations in T_w, EC, and Q at the Bei hot spring were observed in response to changes in precipitation based on daily data (Fig. S1) and the data monitored at 15-minute intervals (Fig. 3). Bei hot spring is replenished by shallow cold water and hot water from thermal reservoir. The shallow cold water exhibits low values of T_w and EC. The T_w and EC values of Bei hot spring showed a significant decreasing trend with increasing precipitation (Fig. S1), indicating that the recharge ratio of shallow cold water had higher. However, the Q at Bei hot spring sometimes increased with precipitation, while at other times, it remained in a dynamically stable state (Fig. S1). This variability was primarily influenced by the operational activities of the Bolian Hotel. The long-term variation curves of T_w, EC, and Q exhibited a pronounced lagged response to precipitation (Fig. S1), which failed to capture the hydrodynamic characteristics of the Bei hot spirng influenced by the precipitation event. Seven distinct precipitation events were identified based on the varation curves of T_w, EC, and Q using the high resolution data (Fig. 3), which could be used to capture the short-term hydrodynamic characterisctis of Bei hot spring. The start time, end time, maximum and minimum values of T_w and EC for each precipitation event (T_{wMax},

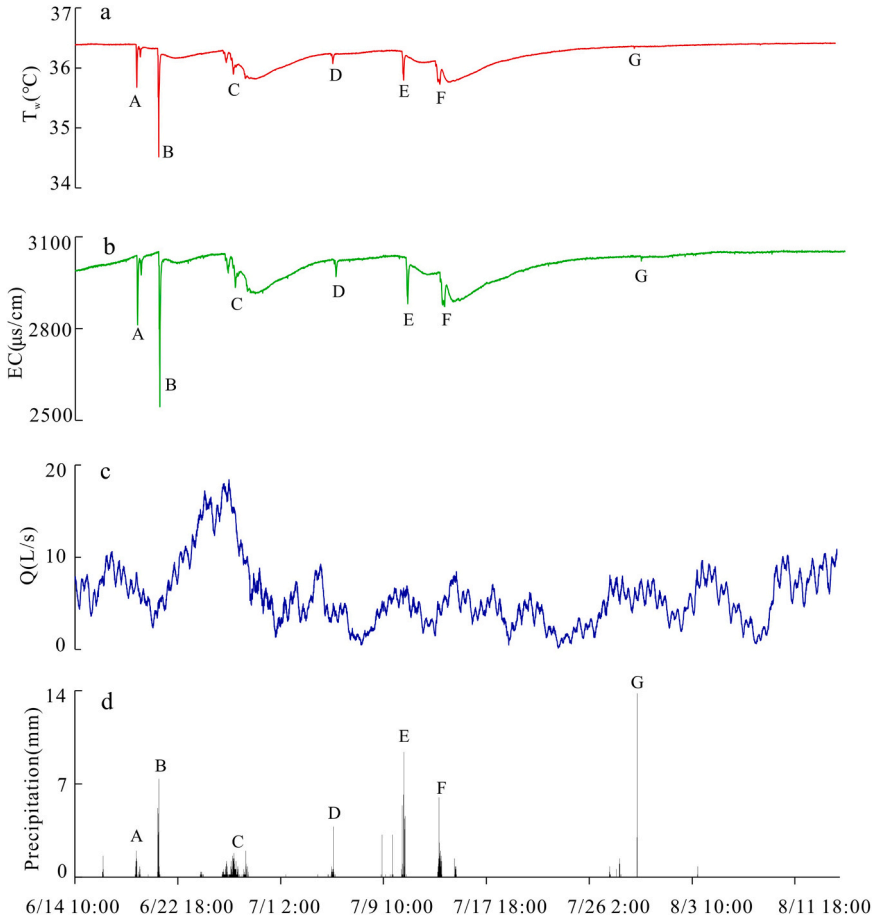

Fig. 3. Variation curves of T_w, EC, and Q in relation to precipitation based on monitoring data collected at 15-minute intervals during the rainy season.

T_{wMin}, EC_{Max}, EC_{Min}), the maximum precipitation recorded in any 15-minute interval (P_{Max}), the total precipitation (P_{Total}), and the precipitation intensity (PI) during the event were presented in Table 1.

The values of T_w and EC exhibited a rapid decreasing trend upon the onset of precipitation (Fig. 3a,b). Once the precipitation ceased, both T_w and EC values increased sharply (Fig. 3a,b). It is crucial to highlight that T_w and EC are sensitive parameters that reflect variations in the hydrodynamic characteristics of the Bei hot spring. The Bei hot spring has been developed into the Bolian hotel. The monitoring location is affected by various external factors, leading to a frequently fluctuating variation curve of Q in the Bei hot spring. However, the increase in Q values from event B (EB) to event C (EC) (Fig. 3c,d) suggested Q values were also influenced by precipitaiton.

The differences between T_{wMax} and T_{wMin} (ΔT), and between EC_{Max} and EC_{Min} (ΔEC) under varying P_{Max} and P_{Total} were depicted in Fig. 4. The variation curves of ΔT_w and ΔEC in relation to different P_{Max} and P_{Total} exhibited significant similarities. The values of ΔT_w and ΔEC initially decreased with increasing P_{Max} (1.4–3.8 mm) and P_{Total} (10.6–13.0 mm), followed by an increase with further increments in P_{Max} (6.0–7.4 mm) and P_{Total} (18.8–37.0 mm). Eventually, they decreased again as P_{Max} (7.4–13.8 mm) and P_{Total} (37.0–63.6 mm) continued to rise. The values of ΔT_w and ΔEC initially increased with PI (from 2.5 mm/h to 9.3 mm/h), and subsequently decreased as PI continued to rise (from 9.3 mm/h to 25.1 mm/h). The maximum values of ΔT_w and ΔEC were recorded during event B, which had a P_{Max} of 7.4 mm, a P_{Total} of 37.0 mm, and a PI of 9.3 mm/h. In contrast, the minimum values of ΔT_w and ΔEC were observed during event G, which had a P_{Max} of 13.8 mm, a P_{Total} of 18.8 mm, and the highest PI of 25.1 mm/h. These findings suggested that the values of ΔT_w and ΔEC were affected by both P_{Max} and P_{Total}.

4.2.2. *Event-scale EC and T_w response*

The hydrograph of karst springs are crucial indicators of karst aquifers. The shape of these hydrographs is influenced by a variety of factors, including the area and morphology of the basin, as well as climatic, hydrological, hydrographic, geological, geomorphological conditions, terrain surface, and vegetation cover.

The curves of T_w, EC, and Q varied with precipitation from Event A to Event D (Fig. 3 and Fig. S1). The hourly variation curves of T_w, EC, and Q during Events A, B, C, and D demonstrated that Events A and D captured the response processes of T_w, EC, and Q to precipitation (Fig. 5 and Fig. S1). The variation curves of T_w, EC, and Q in the Bei hot spring during Events A and D using the hourly data exhibited a rapid response to precipitation (Fig. 5). The values for T_w, EC, and Q in the Bei hot spring at the onset of Event A (2024/6/19 7:15) were 36.39 °C, 3038.4 μs/cm, and 6.61 L/s, respectively. During the precipitation event (Event A), the values of T_w and EC decreased, along with a decline in Q. At the conclusion of the precipitation event on 2024/6/19 at 10:15, the total recorded precipitation was the highest for Event A. At this time, the Bei hot spring exhibited the lowest values of T_w (35.68 °C) and EC (2810.7 μs/cm), while Q reached its peak value of 8.35 L/s (Fig. 5a). When the precipitation ceased, the values of T_w and EC increased, while the Q gradually decreased. The variations in T_w, EC, and Q at the Bei hot spring during Event D exhibited trends similar to those observed during Event A.

The karst aquifer system acts as a filter, producing varied responses and outputs in response to different input signals. Even when the total rainfall from two precipitation events is identical, distinct characteristics in the time series can lead to significantly different output waveforms. The precipitation during Event A demonstrated an initial increase, followed by a subsequent decrease (Fig. 5a), thereby characterizing it as a typical concentrated rainfall event. In contrast, Event D demonstrated a pattern characterized by an initial increase in precipitation, followed by a decline, a subsequent rise, and a final decrease (Fig. 5b). This behavior can be interpreted as two distinct concentrated rainfall events, further supported by the variation curves of T_w and EC, which exhibit two significant low values. The variation curve of Q exhibited a peak value that occurred later than the lowest values of T_w and EC. This suggests that T_w and EC responded more sensitively to precipitation than Q during the complex precipitation event, as further corroborated by the variation curves of Q presented in Fig. 3c. The precipitation process of Event D exhibited more frequent fluctuations than Event A, and the variation curves of T_w, EC, and Q were significantly more diverse compared to those observed in Event A (Fig. 5). The analysis results suggest that the hydrodynamics of the Bei hot spring are closely linked to variations in precipitation. Event A represented a singular precipitation event, and its hydrodynamic analysis more accurately reflects the impact of precipitation. The following research primarily utilized the monitoring data from Event A to analyze the relationships among Q, T_w, and EC, as well as to simulate these elements.

Table 1
Variation of EC and T_w under different precipitation events.

Event	Date		P(mm)			T(°C)		EC(μs/cm)	
	Start	End	P_{Max}	P_{Total}	PI	T_{wMax}	T_{wMin}	EC_{Max}	EC_{Min}
A	6/19 7:30	6/19 10:15	1.4	10.6	3.9	36.40	35.68	3038.4	2810.7
B	6/21 2:15	6/21 6:15	7.4	37.0	9.3	36.33	34.53	3053.0	2545.3
C	6/26 7:30	6/28 10:45	2.0	63.6	19.6	36.30	35.82	3045.8	2913.4
D	7/5 4:30	7/5 9:45	3.8	13.0	2.5	36.24	36.07	3026.1	2969.9
E	7/10 20:15	7/11 3:30	9.4	45.0	6.2	36.28	35.79	3035.0	2880.9
F	7/13 18:30	7/14 3:15	6.0	41.4	4.7	36.12	35.77	2984.9	2877.6
G	7/29 22:30	7/29 23:15	13.8	18.8	25.1	36.37	36.32	3038.6	3020.7

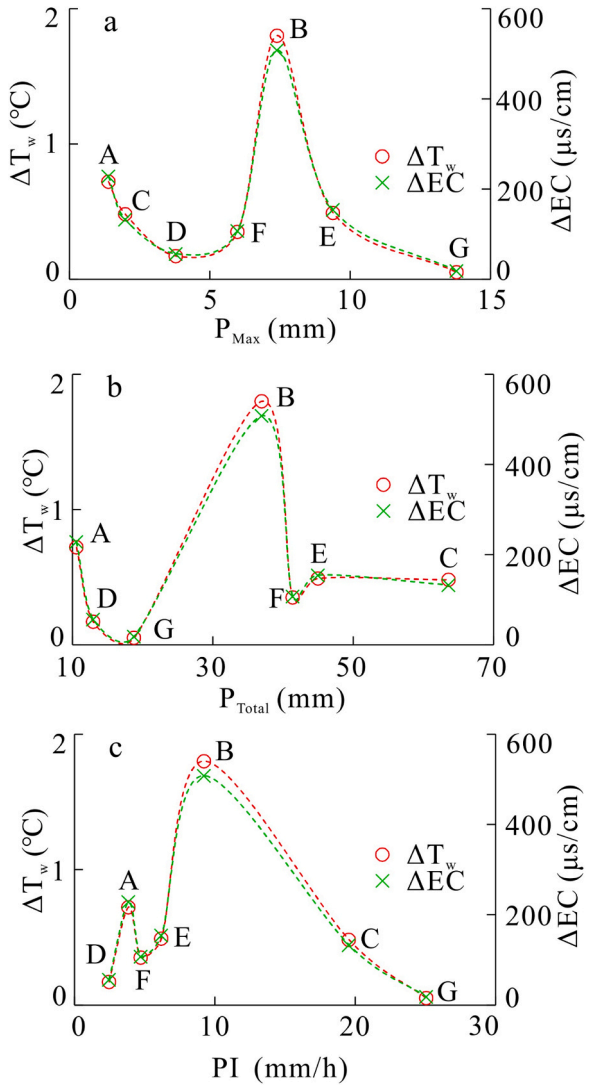

Fig. 4. Variation curves of ΔT and ΔEC with P_{max}, P_{Total} and PI.

4.3. Dynamic variation characteristics of Q, T_w, and EC during the precipitation event

4.3.1. Variation characteristics of Q, T_w, and EC during the recession periods

The precipitation process of Event A is well-suited for analyzing the dynamic variation characteristics of Q, T_w and EC. The variation curves of Q, T_w and EC were plotted in Fig. 6, immediately after the precipitation ceased. The karst hydrological recession curve is influenced by geological, climatic, and topographic factors, providing significant hydrological insights for interpreting the characteristics of aquifer media, hydraulic connections, and the geometric properties of the karst aquifer system (Hall et al., 1968; Amit et al., 2002; Fiorillo et al., 2022; Bonacci and Roje-Bonacci, 2023). Due to the intricate permeability structures of karst aquifers, which encompass conduits, fractures, and matrix (Kogočšek et al., 2023; Musgrove et al., 2023), the recession processes of Q in the Bei hot spring can be distinctly categorized into three stages (Fig. 6a). Therefore, the aquifer associated with the Bei hot spring exemplifies a typical carbonate system.

The hydrograph recession of Q in the Bei hot spring can be represented as the sum of three exponential components, as follows:

$$Q_t = \begin{cases} 10.74e^{-0.078t}I \\ 18.18e^{-0.199t}II \\ 8.65e^{-0.040t}III \end{cases} \tag{23}$$

The recession processes of the conduit, fracture, and matrix correspond to stages I, II, and III, respectively. The recession coefficients for the conduit (α_1), fracture (α_2), and matrix (α_3) were measured to be 0.078, 0.199, and 0.04, respectively. The recession coefficient (α) varies dynamically during the water discharge process and serves as a critical parameter for quantifying the rate of flow

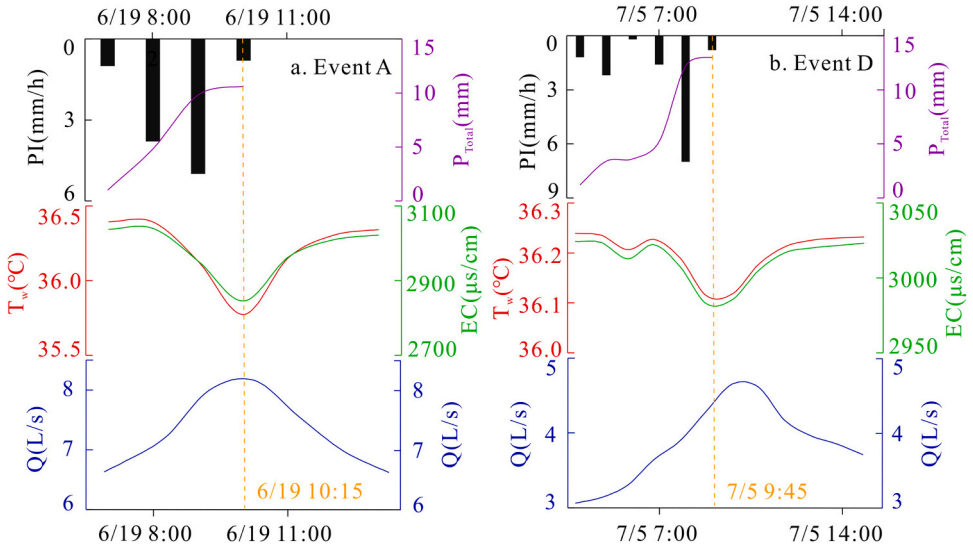

Fig. 5. Variation process of T, EC and Q in the Bei hot spring based on the hourly data collected during the Event A (a) and Event D (b).

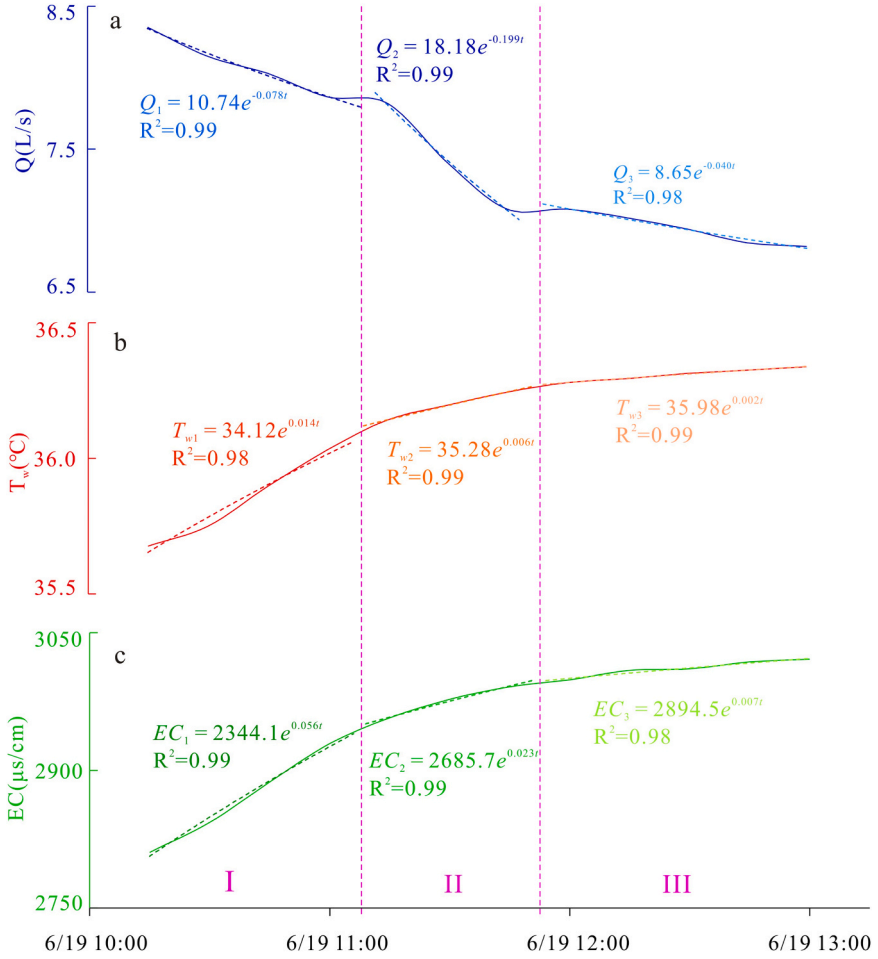

Fig. 6. Variation curves of Q, T_w, and EC immediately after the precipitation Event A ceased.

recession, particularly in relation to karst aquifer media (Guo et al., 2024). The α values of karst water flow generally decrease with increasing duration (Katsanou et al., 2015). However, the value of α_1 is lower than that of α_2, suggesting that the hydraulic connectivity of the conduit is inferior to that of the fracture network. This implies that the conduit is poorly developed in the Bei hot system. The vertical thickness of the Bei hot spring is considerable, with the maximum value of α_2 indicating that the fractures network possesses well-established hydraulic connections. The karst aquifer system is distinguished by its permeability, and the formation of the Bei hot spring typically involves deep circulation processes, as discussed in Section 4.1. The varying dynamics of recession coefficients during the water discharge recession process are indicative of the hydraulic behavior of karst hot springs.

The ratios of conduit water, fracture water, and matrix water were 6.37 %, 8.86 %, and 84.77 %, respectively. The matrix water comprises pore water from shallow cold water and hot water from the geothermal reservoir. Based on the analysis presented in Section 4.1, the ratio of hot water from the geothermal reservoir at Bei hot spring is 78.63 %. Consequently, it can be concluded that the ratio of pore water from shallow cold water is 6.14 %. The conduit water ratio is lower than that of fracture water, further confirming that the conduit system in the Bei hot spring is not well developed. The primary water source of the Bei hot spring is hot water from the geothermal reservoir, which is associated with deep karst water circulation that contributes to the formation of the hot spring.

4.3.2. Conceptual models of recovery processes of EC and T_w

For the Bei hot spring with a specific structure, the values of T_w and EC after a concentrated recharge event are mainly influenced by the volume of the recharge water and the temporal variations in its temperature. The variation curves of T_w and EC exhibited opposite trends compared to Q during the precipitation event (Fig. 5), indicating that the Bei hot spring received a water source characterized by relatively low T_w and EC values. During each recession period of Q, both T_w and EC values increased exponentially (Fig. 6a,b), reflecting the recovery process of these parameters in the Bei hot spring. The three recovery periods were also expressed as the sum of three exponential components as follows:

$$T_{wt} = \begin{cases} 34.12e^{0.014t} I \\ 35.28e^{0.006t} II \\ 35.98e^{0.002t} III \end{cases} \tag{24}$$

$$EC_t = \begin{cases} 2344.1e^{0.056t} I \\ 2685.7e^{0.023t} II \\ 2894.5e^{0.007t} III \end{cases} \tag{25}$$

The conceptual models of recovery processes of EC and T_w in the Bei hot spring were constructed in the following based on the above exponential equations:

$$N_t = \begin{cases} N_1 e^{\lambda_1 t}[0, t_1) \\ N_2 e^{\lambda_2 t}[t_1, t_2) \\ N_3 e^{\lambda_3 t}[t_2, t_3) \end{cases} \tag{26}$$

Where N_1, N_2, and N_3 represent the initial values of T_w or EC in the conduit, fracture, and matrix at the onset of Q's recession, respectively; λ_1, λ_2 and λ_3 denote the recovery coefficients of T_w or EC in the conduit, fracture, and matrix, respectively.

The recovery coefficient (λ) is a crucial parameter for quantifying the variation rates of T_w and EC. The values for λ_{Tw1}, λ_{Tw2}, and λ_{Tw3} were 0.014, 0.006, and 0.002, respectively. Likewise, the values of λ_{EC1}, λ_{EC2}, and λ_{EC3} were 0.056, 0.023, and 0.007, respectively. The recovery coefficient (λ) exhibited a decreasing trend during the recovery process of T_w and EC. In contrast to the variation characteristics of the recession coefficient (α) of Q, the recovery coefficient (λ) is particularly related to the values of T_w and EC from water sources. The variation ranges of T_w and EC in conduit water were greater than those observed in the fracture water and matrix water. Matrix water exhibited the most stable values for T_w and EC. Therefore, analyzing the relationships among T_w, EC, and Q is essential for evaluating the water resources of Bei hot spring.

4.3.3. Dynamic correlations among Q, T_w, and EC during the precipitation event

Both the recession of Q and the recovery of T_w/EC adhered to an exponential model during each period (Fig. 6). The mathematical equations among Q, T_w, and EC were analyzed and are presented as follows:

$$Q_t = \begin{cases} -1.26T_w + 53.45(R^2 = 0.95) I \\ -7.19T_w + 267.78(R^2 = 0.99) II \\ -4.66T_w + 176.13(R^2 = 0.98) III \end{cases} \tag{27}$$

$$Q_t = \begin{cases} -0.004EC + 19.36(R^2 = 0.98) I \\ -0.022EC + 72.28(R^2 = 0.99) II \\ -0.012EC + 43.94(R^2 = 0.94) III \end{cases} \tag{28}$$

$$EC_t = \begin{cases} 325.69T_w - 8804.6(R^2 = 0.99) I \\ 329.06T_w - 8934.8(R^2 = 0.99) II \\ 360.09T_w - 10063(R^2 = 0.94) III \end{cases} \tag{29}$$

There exists a distinct linear relationship among Q, T_w, and EC throughout each period. The linear equations demonstrate that the

specific volume of Q is associated with special values of T_w and EC. The absolute slope values (k) for Q and T_w, as well as Q and EC, were highest during the second period (II). Furthermore, the slope values (k) for EC and T_w demonstrated an increasing trend from the first period (I) to the third period (III). This observation further confirmed the unique hydrogeological structure of the Bei hot spring. Using the aforementioned linear relationships, the values of T_w and EC in conduit water, fracture water, and matrix water, along with the corresponding ratios of these water sources, can be quantitatively determined.

The third phase (III) represents the process of matrix water recession. It can be concluded that the volume of matrix water ranges from 6.84 L/s to 7.08 L/s. The values of T_w and EC ranged from 36.28 °C to 36.34 °C and from 2998.4 μs/cm to 3020.9 μs/cm, respectively. The measurements for Q, T_w, and EC during the transition of fracture water to matrix water were found to be 7.08 L/s, 36.28 °C, and 2998.4 μs/cm, respectively. Utilizing the linear relationships among Q, T_w, and EC for each period, the variation ranges of T_w and EC in fracture water were found to be 34.29–34.82 °C and 2488.51–2560.92 μs/cm, respectively. In conduit water, the variation ranges of T_w and EC were 26.43–28.85 °C and 136.01–662.03 μs/cm, respectively. The average values of T_w in conduit water, fracture water, and matrix water were 27.34, 34.56, and 36.31 °C, respectively. The average values of EC in conduit water, fracture water, and matrix water were 358.03, 2524.72, and 3011.22 μs/cm, respectively. The values of T_w and EC in conduit water were significantly lower than those in fracture water and matrix water. Specifically, the EC values in matrix water and fracture water were 8.4 and 7.05 times greater than those of conduit water, respectively. This indicates that the conduit is situated within a shallow karst aquifer system. During the precipitation Event A, the average air temperature (T_{Air}) was recorded at 27.65 °C, which closely matched the temperature of the conduit water, further confirming that the conduit is poorly developed in the shallow karst aquifer system.

4.4. Simulations of Q, T_w, and EC in the Bei hot spring

4.4.1. The precipitation infiltration coefficient (α) of the Bei hot spring

The infiltration rate (α) is defined as the ratio of groundwater recharge from a specific amount of precipitation to the total precipitation received in a given catchment area (Al-humair et al., 2023). The outlet of the Bei hot spring collects the region's water resources, with water level automatically monitored using the Solinst Levelogger 4.6.2. LTC (Canada) in a marshall tank at 15-min intervals. The groundwater discharge, influenced by infiltraion at the Bei hot spring, is reflected in the changes in water level at the outlet (ΔH_w). According to the Eq. (11), the precipitation infiltration coefficient (α) is defined as the ratio of ΔH_w to P. Therefore, the equation can be expressed as follows: $\alpha = \Delta H_w/P$. The values of α fluctuated throughout the precipitation process due to factors such as soil moisture, surface vegetation, evaporation, topographic slope. The characterisctis of α during the precipitaiton Event A were depicted in Fig. 7.

The values of α corresponding to hourly precipitation levels of 1.0 mm, 3.8 mm, 5.0 mm, and 0.8 mm were 0.013, 0.005, 0.003, and 0.016, respectively. The values of α exhibited a clear negative linear trend with the amount of precipitaiton ($y = -0.003x + 0.02$, R^2=0.98). Therefore, it can be concluded that a higher volume of precipitation is likely to produce increased surface water flow, whereas a lower volume of precipitation may infiltrate the Bei hot spring system at a reduced rate. Consequently, the infiltration rate can be determined from the variations in water levels at the outlet during the precipitation event. This finding offers valuable insights for deriving hydrological parameters from hydrographs, which can subsequently be used to evaluate the water resources of the karst aquifer system.

4.4.2. Simulations of Q, T_w, and EC during the precipitation event at the Bei hot spring

The hydrological and hydrochemical factors of Q, T_w, and EC responded rapidly to precipitation during the Event A, indicating that precipitation was the primary factor influencing hydrodynamics and hydrochemistry in the Bei hot spring. The phenomenon suggested that simulating the dynamic variations of Q, T_w, and EC in the Bei hot spring during the Event A was appropriate.

The value of τ is influenced by the shape and response time of the hydrograph curve, which can be derived from the measured hydrograph. It functions as a lumped parameter representing the structure of the karst aquifer system, encapsulating both the scale of the aquifer and the characteristics of the aquifer media. The value of τ was determined to be 2.50 h based on the hydrograph curves of Q during Event A. The total hydrograph represents the cumulative sum of all calculated hydrograph elements. It can be inferred that the values of M varied according to the Eq. (16), with a range of variation from 26.25 m^2/s to 58.41 m^2/s. The simulation that best

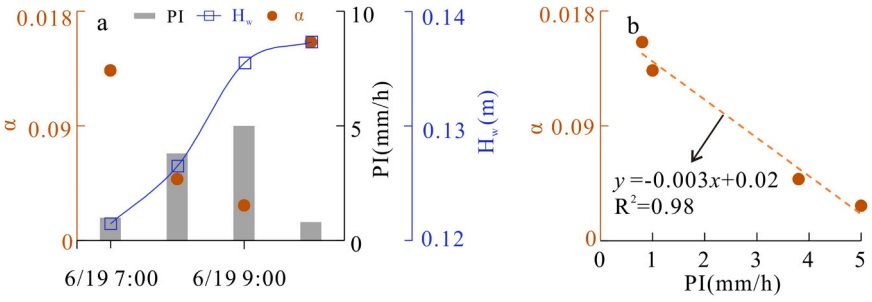

Fig. 7. Variation characteristics of α in relation to precipitation levels (a: values of α and H_w across different PI; b: the linear relationship between α and PI).

represents the observed water discharge was shown in Fig. 8a, as evidenced by the highest values of the NSE at 0.96 and the VE at 0.99.

It can be inferred from Eqs. (23)–(25) that T_w and EC were in the recovery period, while Q was in the recession period. Additionally, Eqs. (27) and (28) indicated that Q exhibited negative linear relationships with both T_w and EC. Therefore, the dynamics of T_w and EC exhibited opposite variations compared to Q. The hydrological pulse simulation model was also effective in simulating T_w and EC. Finally, the best simulations of the observed T_w and EC were shown in Fig. 8b and c, where both the NSE and VE values approached 1, indicating the appropriateness of the simulation model. Therefore, the hydrological pulse model is invaluable for predicting variations in the hydrograph and hydrochemograph of Bei Hot Spring under natural conditions. Ultimately, the mathematical equation for the hydrochemograph pulse model can be formulated as follows:

$$N_t = N_0 + \sum_{i=1}^{m} \Delta N_i \left(\frac{2e\tau}{3t}\right)^{1.5} e^{-\tau/t} \tag{30}$$

Where N_t represents the value of T_w or EC at time t, N_0 denotes the value of T_w or EC at the onset of the precipitation event, and m signifies the number of precipitation events.

The simulation results of the pulse model clearly demonstrate the processes of variation for Q, T_w, and EC. The τ and M parameters were derived from these simulations, which are crucial for evaluating the water resources of Bei hot spring.

The values of α, τ, and M could be derived from the fluctuations in water levels during the precipitation event and the simulation processes of the pulse model. Consequently, the area of Bei hot spring (A) could be calculated using the Eq. (18), resulting in a value of 67.87 km^2. Thus, the water discharge (Q) of Bei hot spring under natural conditions can be evaluated using the Eq. (15).

4.5. Hydrogeological genetic model for the Bei hot spring

The axial parts and two wings of each anticline expose the Triassic strata, which can be classified from oldest to youngest as follows: the Feixianguan Formation (T_1f), the Jialingjiang Formation (T_1j), the Leikoupo Formation (T_2l), and the Xujiahe Formation (T_3xj). The T_1f formation primarily consists of shale and mudstone, and exhibiting water barrier characteristics. It serves as the bottom layer for the geothermal reservior (Fig. 9). The T_1j formation primarily consists of limestone, dolomite, bioclastic rocks, and gypsum-salt breccia. This formation acts as a geothermal reservoir and is located in the near-axis region of anticlines. The carbonates in T_1j

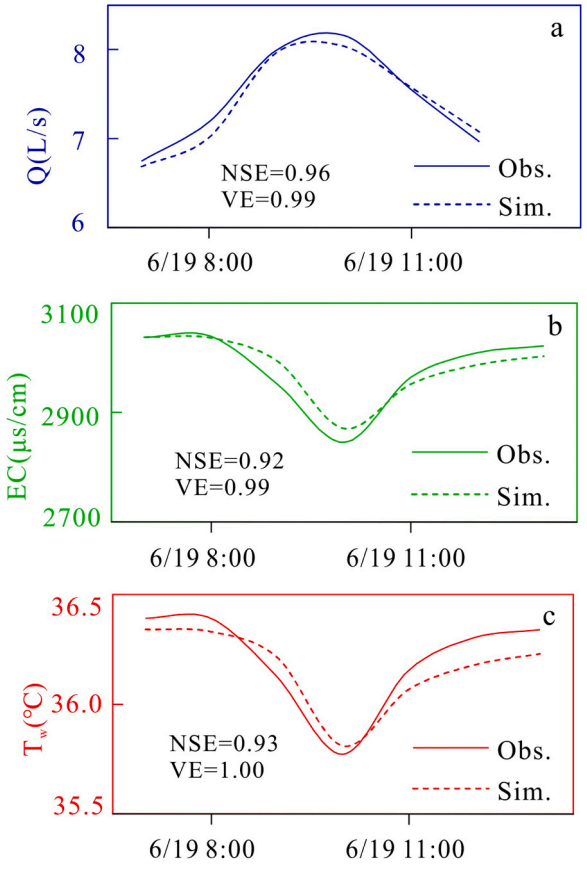

Fig. 8. The simulation results of Q, EC and Tw in the Bei hot spring using the theoretical model.

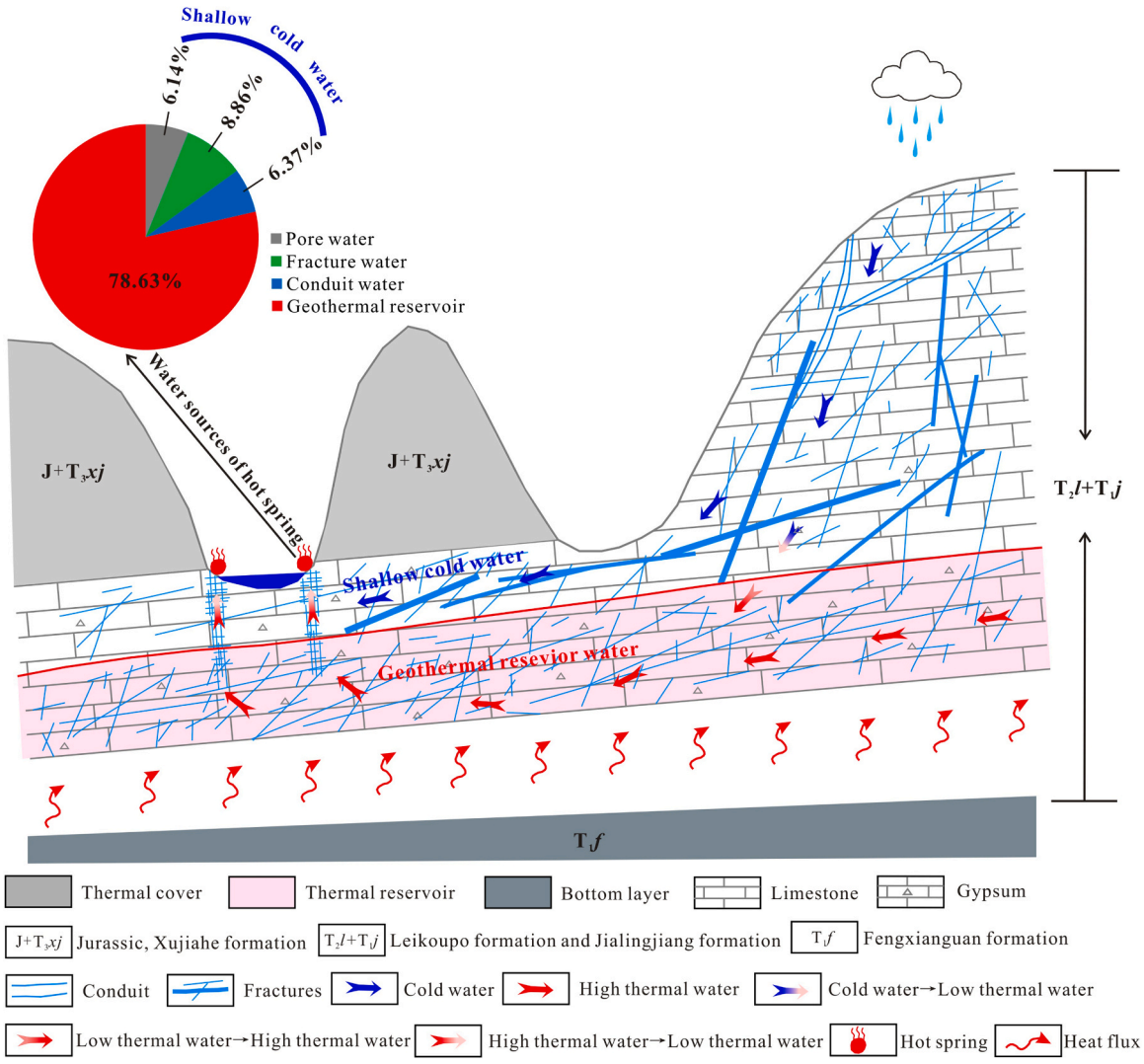

Fig. 9. Hydrogeological genetic model for the formation of thermal water in Bei hot spring.

formation show well-developed karst conduits and corrosion, which imply a good geothermal reservoir (Fig. 9). The T_2l formation primarily consists of dolomite, limestone, and claystone. The formation is distributed in a linear pattern along the wings of the WTX anticline, therby contributing to the geothermal reservoir. The T_3xj formation and the Jurassic strata serve as the geothermal cover for the geothermal reservoir (Fig. 9). The T_3xj formation is mainly characterized by sandstone, shale interbedded with thin coal seams.

The recharge ratios of shallow cold water and hot water from the geothermal reservoir were 21.37 % and 78.63 %, respectively (Fig. 9). The hydrodynamics of the Bei hot spring are closely linked to the variations in precipitation, primarily due to the shallow water flow paths of cold water. As a result, both T_w and EC respond sensitively to changes in precipitation. Although the Q is influenced by the operational activities of the Bolian Hotel, the hydrodynamic of Q remain relativley stable, as the hot spring is primarily replenished by the geothermal reservior. The EC values in the conduit water were significantly lower than those in the fracture water and matrix water. This indicated that the conduit is poorly developed in the upper part of Bei hot system. Therefore, the temperature of the conduit water was similar to that of the surrounding air. The highest recession coefficient of fracture water indicated that the fracture network has well-established hydraulic connections and served as the primary vertical pathway for precipitation to flow into the carbonate thermal reservoir. The recession process of Q and the recovery processes of EC and T_w in the Bei hot spring followed exponential equations. The hydrological pulse model effectively simulated the variation processes of Q, T_w, and EC under natural conditions, indicating that the hydrodynamic and hydrochemistry of the Bei hot spring are primarily governed by the carbonate aquifer system.

Precipitation infiltrates karst outcrop regions situated within the parallel ridge and valley anticlinal structures of eastern Sichuan and the northern Huaying mountains. Shallow pores and conduits receive precipitation, which accumulates in the well-connected fracture network. In the upper part of the system, the collected water flows through the geological strata, forming shallow cold

water. Vertically, this water moves downward, with groundwater temperatures increasing with depth, eventually entering the geothermal reservoir and resulting in the geothermal water source of the Bei hot spring. Water flow reaches depths ranging from approximately 2.61 to 5.42 km, with the thermal reservoir temperature varying between about 72.00 and 127.36 °C. The thermal water rises to the surface through fractures along faults in the deep valley.

5. Conclusions

In this study, we analyzed the dynamic variation processes of natural tracers, calculated the proportions of various water sources, developed the simulation model for Q, T_w, and EC during a single precipitation event and the hydrogeological conceptual model of the Bei hot spring. The main conclusions are summarized below.

(1) T_w and EC are sensitive natural tracers, exhibited clear negative linear relationships with Q during the single precipitation event, in the absence of the operational activities of the Bolian Hotel. The variation curves of T_w and EC The values of ΔT and ΔEC during the precipitation were influenced by both P_{Max} and P_{Total}.

(2) The Bei hot spring is primarily replenished by hot water from the geothermal reservoir (78.63 %), followed by shallow cold water (21.37 %). The proportions of pore water, fracture water, and conduit water of shallow cold water were 6.14 %, 8.86 %, and 6.37 %, respectively.

(3) The mathematical recovery model for EC or T_w was developed based on the inverse relationships among T_w, EC, and Q. The hydrological and hydrochemical pulse model successfully simulated the dynamic variation of T_w, EC, and Q during a single precipitaiton event, and calculated the precipitation infiltration coefficient (α) and the catchment area (A).

(4) Hydrogeological genetic model of Bei hot spring was constructed by intergrating the hydrodynamics of shallow cold water, the spatial geological structure of geothermal reservoir, and the recharge characteristics of water sources.

These findings not only elucidated the dynamic characteristics of Q, T_w and EC during the single precipitation event, but also had significant implications for the calculation of hydrogeological parameters and the assessment of water sources in karst hot spring. The research findings will assist the Chongqing Bureau of Planning and Natural Resources in implementing strategies to ensure the sustainable development of geothermal water resources.

CRediT authorship contribution statement

Fuxiang Chi: Methodology, Software, Conceptualization, Investigation. **Yongli Guo:** Investigation, Project administration, Resources, Conceptualization, Writing – original draft, Methodology. **Matej Blatnik:** Writing – review & editing, Supervision, Conceptualization, Methodology. **Qiong Xiao:** Project administration, Conceptualization, Supervision, Methodology, Investigation.

Declaration of Competing Interest

The authors declare that they have no known competing financial interests or personal relationships that could have appeared to influence the work reported in this paper.

Acknowledgments

Financial support was provided by the National Natural Science Foundation of Guangxi Province (2023GXNSFAA026473, GuikeAB25069498), National Key Research and Development Program of China (2020YFE0204700), Fundamental Scientific Research Funds of Institute of Karst Geology, CAGS (2023019), China Geological Survey Project (DD20230547) and National Natural Science Foundation of China (42261144672). The authors would like to thank Qiufang He, Yifei Liu, Ning Zhang, and Licheng Shen for their assistance in fieldwork.

Appendix A. Supporting information

Supplementary data associated with this article can be found in the online version at doi:10.1016/j.ejrh.2025.102613.

Data availability

Data will be made available on request.

References

Al-humair, B.A.J., Rahal, N.S., Alalwan, H.A., 2023. Studying the effect of climate elements variability on surface water runoff and infiltration rate in Babylon province by using statistical analysis. Int. J. Hydrol. Sci. Tec. 16 (2), 107–121. https://doi.org/10.1504/IJHST.2023.132584.

Amit, H., Lyakhovsky, V., Katz, A., Starinsky, A., Burg, A., 2002. Interpretation of spring recession curves. Groundwater 40 (5), 543–551.

Bailly-Comte, V., Martin, J.B., Jourde, H., Screaton, E.J., Pistre, S., Langston, A., 2010. Water exchange and pressure transfer between conduits and matrix and their influence on hydrodynamics of two karst aquifers with sinking streams. J. Hydro. 386, 55–66. https://doi.org/10.1016/j.jhydrol.2010.03.005.
Birk, S., Liedl, R., Sauter, M., 2004. Identification of localised recharge and conduit flow by combined analysis of hydraulic and physico-chemical spring responses (Urenbrunnen, SW-Germany). J. Hydrol. 286 (1–4), 179–193. https://doi.org/10.1016/j.jhydrol.2003.09.007.
Bonacci, O., Roje-Bonacci, T., 2023. Water temperature and electrical conductivity as an indicator of karst aquifer: the case of Jadro Spring (Croatia). Carbonate Evaporite 38, 55. https://doi.org/10.1007/s13146-023-00881-x.
Criss, R.E., Winston, W.E., 2008. Discharge predictions of a rainfall-driven theoretical hydrograph compared to common models and observed data. Water Resour. Res. 44, 10407. https://doi.org/10.1029/2007WR006415.
Cui, W., Quan, L., Chang, G., Chen, G., Jen, T.C., 2011. Measurement and prediction of undisturbed underground temperature distribution. Int. Mech. Eng. Congr. Expo. https://doi.org/10.1115/IMECE2011-63311.
Fiorillo, F., Pagnozzi, M., Addesso, R., Cafaro, S., D'Angeli, I.M., Esposito, L., Leone, G., Liso, I.S., Parise, M., 2022. Uncertainties in understanding groundwater flow and spring functioning in karst. In: Currell, M.J., Katz, B.G. (Eds.), Threats to Springs in a Changing World: Science and Policies for Protection. American Geophysical Union, Washington DC, pp. 131–143. https://doi.org/10.1002/9781119818625.ch9.
Ford, D., Williams, P.D., 2013. Karst hydrogeology and geomorphology. John Wiley & Sons.
Fournier, R., 1977. Chemical geothermometers and mixing models for geothermal systems. Geothermics 5, 41–50. https://doi.org/10.1016/0375-6505(77)90007-4.
Goswami, S., Rai, A.K., 2025. Geothermal energy is a ubiquitous, sustainable, and scientifically feasible resource among other renewable energy sources. J. Clean. Prod. 512, 145637. https://doi.org/10.1016/j.jclepro.2025.145637.
Grasby, S.E., Ferguson, G., Bartier, P., Neville, L., 2019. Seismic induced flow disruption of Gandll K'in Gwaay.yaay thermal springs, Gwaii Haanas National Park Reserve, Canada. Appl. Geochem 103, 118–130. https://doi.org/10.1016/j.apgeochem.2019.03.005.
Guo, X.L., Chen, Q.L., Huang, H., Wang, Z.J., Li, J.W., Huang, K., Zhou, H., 2022. Water source identification and circulation characteristics of intermittent karst spring based on hydrochemistry and stable isotope — An example from Southern China. Appl. Geochem. 141, 105309. https://doi.org/10.1016/j.apgeochem.2022.105309.
Guo, Y.L., Huang, F., Chi, F.X., Zhang, N., Ma, J., Miao, Y., Chen, F.J., 2024. Hydrogeological stuctures of karst features using hydrographs in an underground river basin formed in a peak cluster depression, southwest China. J. Hydrol. (634), 131085. https://doi.org/10.1016/j.jhydrol.2024.131085.
Guo, Y.L., Huang, F., Sun, P.A., Zhang, C., Xiao, Q., Wen, Z., Yang, H., 2023. Hydrogeological functioning of a karst underground river basin in southwest China. Groundwater 61 (6), 895–913. https://doi.org/10.1111/gwat.13361.
Hall, F.R., 1968. Base flow recessions: a review. Water Resour. Res. 4 (5), 973–983. https://doi.org/10.1029/WR004i005p00973.
Herms, I., Jódar, J., Soler, A., Vadillo, I., Lambán, L.J., Martos-Rosillo, S., Nunez, J.A., Arno, G., Jorge, J., 2019. Contribution of isotopic research techniques to characterize high-mountain-Mediterranean karst aquifers: the Port del Comte (Eastern Pyrenees) aquifer. Sci. Total Environ. 656, 209–230. https://doi.org/10.1016/j.scitotenv.2018.11.188.
Katsanou, K., Lambrakis, N., Tayfur, G., Baba, A., 2015. Describing the karst evolution by the exploitation of hydrologic time-series data. Water Resour. Manag. 29 (9), 3131–3147. https://doi.org/10.1007/s11269-015-0987-x.
Kogočšek, B., Jemcov, I., Petrič, M., 2023. Advanced application of time series analysis in complex karst aquifers: a case study of the Unica springs (SW Slovenia). J. Hydrol. 626, 130147. https://doi.org/10.1016/j.jhydrol.2023.130147.
Lauber, U., Kotyla, P., Morche, D., Goldscheider, N., 2014. Hydrogeology of an Alpine rockfall aquifer system and its role in flood attenuation and maintaining baseflow. Hydro. Earth Syst. Sci. 18, 4437–4452. https://doi.org/10.5194/hess-18-4437-2014.
Li, D., Liu, D., 2011. Geothermal reservoir structure and runoff flow recharge of geothermal water resources in Chongqing City. J. Hohai Univ. (Nat. Sci.) 39 (4), 372–376. https://doi.org/10.3876/j.issn.1000-1980.2011.04.004 (in Chinese with English abstract).
Li, L., Tang, Y.E., Yang, Y., Ye, X.C., Kong, Z.G., 2025. Characteristics of groundwater circulation in typical karst trough areas: a case study of Longtan trough valley in Youyang. Chongqing Hydrogeol. Eng. Geol. 52 (2), 53–62. https://doi.org/10.16030/j.cnki.issn.1000-3665.202403044 (in Chinese with English abstract).
Li, N., Zhou, H., Wen, Z., Jakada, H., 2019. Formation mechanism and mixing behavior of Nanyang thermal spring, Xingshan county of Hubei Province, central China. Hydrogeol. J. 27, 2933–2953. https://doi.org/10.1007/s10040-019-02041-9.
Luhmann, A.J., Covington, M.D., Alexander, S.C., Chai, S.Y., Schwartz, B.F., Groten, J.T., Alexander Jr, E.C., 2012. Comparing conservative and nonconservative tracers in karst and using them to estimate flow path geometry. J. Hydrol. 448, 201–211. https://doi.org/10.1016/j.jhydrol.2012.04.044.
Luo, M.M., Chen, Z.H., Criss, R.E., Zhou, H., Jakada, H., Shi, T.T., 2016. Method for calibrating a theoretical model in karst springs: an example for a hydropower station in South China. Hydrol. Process 30, 4815–4825. https://doi.org/10.1002/hyp.10950.
Luo, M.M., Jiang, G.H., 2022. Estimation method of recharge area based on hydrograph simulation of karst water. Bull. Geol. Sci. Technol. 41 (5), 293–300, 10.19509.cnki.dzk.2022.0184. (in Chinese with English abstract).
Luo, M.M., Wan, L., Liao, C.L., Jakada, H., Zhou, H., 2023. Geographic and transport contols of temperature response in karst springs. J. Hydrol. 623, 129850. https://doi.org/10.1016/j.jhydrol.2023.129850.
Ma, J.R., Zhou, J., Wu, Y.Q., Zhuo, L.Y., Wang, M.M., Liu, Y., Xu, H.F., Wang, Y.X., Tao, G.B., Cui, J.W., Wang, C., 2024. Characterization of hydrogeochemistry of the hot springs on both sides of the Nujiang River near Baoshan in the Yunnan-Tibet Geothermal Belt. J. Hydrol. Reg. Stud. 56, 102055. https://doi.org/10.1016/j.ejrh.2024.102055.
Maillet, E., 1905. Essais d'Hydraulique souterraine et fluviale [Underground and River Hydrology]. Hermann, Paris, 218.
Musgrove, M., Jurgens, B.C., Opsahl, S.P., 2023. Karst groundwater vulnerability determined by modeled age and residence time tracers. Geophys. Res. Lett. 50, 102853. https://doi.org/10.1029/2023GL102853.
Na, J., Cen, C., Shi, Z.M., Feng, B., 2024. Distinct response of deep and shallow geothermal reservoir temperature following earthquakes in the Kangding Fault zone hydrothermal system. J. Hydrol. Reg. Stud. 52, 101743. https://doi.org/10.1016/j.ejrh.2024.101743.
Nash, J.E., Sutcliffe, J.V., 1970. River flow forecasting through conceptual models: part 1– A discussion of principles. J. Hydrol. 10, 282–290. https://doi.org/10.1016/0022-1694(70)90255-6.
Petrović, B., Marinović, V., 2023. Quantitative and Geochemical Characterization of the Mokra Karst Aquifer (SE Serbia) by Time Series Analysis and Stochastic Modelling. In: EuroKarst 2022, Málaga: Advances in the Hydrogeology of Karst and Carbonate Reservoirs. Springer International Publishing, Cham, pp. 49–55.
Pinza, J.G., Katsanou, K., Lambrakis, N., Stigter, T., 2024. Temporal variations of spring hydrochemistry as clues to the karst system behaviour: an example of Louros catchment. Environ. Monit. Assess. 196, 624. https://doi.org/10.1007/s10661-024-12744-6.
Schaper, J.L., Cirpka, O.A., Lewandowski, J., Zarfl, C., 2024. Electrical conductivity fluctuations as a tracer to determine time-dependent transport characteristics in hyporheic sediments. J. Hydrol. 643, 131914. https://doi.org/10.1016/j.jhydrol.2024.131914.
Shi, W.G., Zhan, H.B., Wang, Q.R., Liao, Z.L., 2024. Quantifying vertical streambed fluxex and streambed thermal properties using heat as a tracer during exteme hydrologic events. J. Hydrol. 629, 130553. https://doi.org/10.1016/j.jhydrol.2023.130553.
Shuster, E.T., White, W.B., 1971. Seasonal fluctuations in the chemistry of limestone springs: a possible means for characterizing karst aquifers. J. Hydro. 14 (2), 93–128. https://doi.org/10.1016/0022-1694(71)90001-1.
Ta, M.M., Zhou, X., Guo, J., Wang, X.Y., Wang, Y., Xu, Z.P., 2018. Occurrence and formation of the hot springs and thermal groundwater in Chongqing. Hydrogeol. Eng. Geol. 45 (1), 165–172. https://doi.org/10.16030/j.cnki.issn.1000-3665.2018.01.24 (in Chinese with English abstract).
Verma, S.P., Santoyo, E., 1997. New improved equations for Na/K, Na/Li and SiO_2, geothermometers by outlier detection and rejection. J. Volcanol. Geotherm. Res. 79, 9–23. https://doi.org/10.1016/S0377-0273(97)00024-3.
Wang, F., Chen, H.S., Lian, J.J., Fu, J.J., Fu, Z.Y., Nie, Y.P., 2020. Hydrological response of karst stream to precipitation variation recognized through the quantitative separation of runoff components. Sci. Total Environ. 728, 142483. https://doi.org/10.1016/j.scitotenv.2020.142483.
Wang, J.Y., Xiong, L.P., Pang, Z.H., 1993. Medium-Low Temperature Convective Geothermal System. Science Press, Beijing, pp. 117–132 (in Chinese).

Wang, Y.W., Zhou, X.C., Li, J.C., Bai, Y.F., Yan, Y.C., Jiao, T., He, M., Zeng, Z.J., Yao, B.Y., Xing, G.Y., Cui, S.H., Li, Y., Li, L.W., 2025. Hydrogeochemical characteristics of hot springs in the Longriba fault, northeastern Tibetan Plateau: tectonic implications for geothermal fluid circulation. J. Asian Earth Sci. 281, 106511. https://doi.org/10.1016/j.jseaes.2025.106511.

Wei, Z.G., Huang, S.P., Xu, J.W., Yuan, C., Zhang, M., Wang, C.S., 2024. Geochemical evolution of geothermal waters in the Pearl River Delta region, South China: insights from water chemistry and isotope geochemistry. J. Hydrol. Reg. Stud. 51, 101670. https://doi.org/10.1016/j.ejrh.2024.101670.

Winston, W.E., Criss, R.E., 2004. Dynamic hydrologic and geochemical response in a perennial karst spring. Water Resour. Res. 40 (5), W05106. https://doi.org/10.1029/2004WR003054.

Xiao, Q., 2012. Water-Rock Interaction and Genesis of Thermal Groundwater in Carbonate Reservoir in Chongqing. Southwest University (PhD thesis. (in Chinese with English abstract)).

Xiao, Q., Jiang, Y.J., Shen, L.C., Yuan, D.X., 2018. Origin of calcium sulfate-type water in the Triassic carbonate thermal water system in Chongqing, China: a chemical and isotopic reconnaissance. Appl. Geochem. 89, 49–58. https://doi.org/10.1016/j.apgeochem.2017.11.011.

Yang, P.H., Cheng, Q., Xie, S.Y., Wang, J.L., Chang, L.R., Yu, Q., Zhan, Z.J., Chen, F., 2017. Hydrogeochemistry and geothermometry of deep thermal water in the carbonate formation in the main urban area of Chongqing, China. J. Hydrol. 549, 50–61. https://doi.org/10.1016/j.jhydrol.2017.03.054.

Yang, Y., Endreny, T.A., 2013. Watershed hydrograph model based on surface flow diffusion. Water Resour. Res. 49, 507–516. https://doi.org/10.1029/2012WR012186.

Yuan, J.F., Liu, H.Z., Deng, G.S., Li, M.H., 2022. Structural characteristics of Triassic carbonate geothermal reservoir and genesis of thermal water in the Tongluo mountain anticline of Guang'an City, China. Carsol. Sin. 41 (4), 623–635. https://doi.org/10.11932/karst20220410 (in Chinese with English abstract).

Zhang, H., He, R.S., Kang, X.B., Yang, Y.B., Li, Q., Gao, Y., Zhou, J.R., Chai, J.L., 2024. Characteristics of the underground hot water circulation system western Yunnan Yingjiang basin and resources development potential. Carsol. Sin. 43 (6), 1317–1326. https://doi.org/10.11932/karst20240609 (in Chinese with English abstract).

Zhang, J.R., Yang, P.H., Groves, C., Luo, X.H., Wang, Y.Y., 2022. Influence of geological structure on the physicochemical properties and occurrence of middle-deep groundwater in Chongqing, Southwest China. J. Hydrol. 610, 127782. https://doi.org/10.1016/j.jhydrol.2022.127782.